


Research Article

Stress Characteristics near Wellbore and Prevention Casing Deformation for Fracturing Horizontal Wells

Peng Zhang,^{1,2} Zhenghua Wu,² Shuying Hu,³ Jikai Wei,² Manlai Zhang,⁴ Zhengqin Ye,⁵ Chunsheng Pu¹ ,¹ and Jingyang Pu¹

¹School of Petroleum Engineering, China University of Petroleum (East China), Qingdao 266580, China

²TUHA Petroleum Research & Development Center, Hami, Xinjiang 839009, China

³TUHA New Energy Center, Hami, Xinjiang 839009, China

⁴Gas Lift Innovation Center, Laboratory of Multiphase Pipe Flow, Yangtze University, CNPC, Wuhan 430100, China

⁵Yanchang Oilfield Co., Ltd., Yan'an, Shaanxi 716000, China

Correspondence should be addressed to Chunsheng Pu; chshpu@163.com

Received 5 October 2022; Revised 4 December 2022; Accepted 13 December 2022; Published 30 December 2022

Academic Editor: Jinze Xu

Copyright © 2022 Peng Zhang et al. This is an open access article distributed under the Creative Commons Attribution License, which permits unrestricted use, distribution, and reproduction in any medium, provided the original work is properly cited.

Aiming at the problem that casing deformation can easily occur in tight oil horizontal well fracturing, based on the rock mechanics experiments and probability statistics, the distribution characteristics and law of the near-wellbore stress field of the reservoir in STH M56 were solved and analyzed by using the finite element modeling numerical method. The research shows that (1) the max/min horizontal stress ratio of the M56 tight oil reservoir is 1.2, the difference is less than 8 MPa, and this characteristic condition is more conducive to the formation of complex fracturing network in the reservoir during fracturing. (2) In M56, the Mises stress isoline near the borehole is symmetrically distributed. Stress concentration has four dangerous points (30°, 150°, 210° and 330°); a sector-shaped high dangerous stress zone is formed along the four dangerous points. As the pumping pressure increases, the vertical Mises stress first increases and then decreases, while the horizontal Mises stress first decreases and then increases. The max-Mises stress at the casing wall is linearly and positively correlated with the stress uniformity coefficient. When the pumping pressure is 80 MPa, the Mises stress exceeds the safe pressure limit of the casing. A pumping pressure of 70 MPa fracturing is the safe pumping pressure for the reservoir casing. (3) It is found that the 90° and 270° horizontal fixed plane perforations can avoid the dangerous stress zone, increasing and decreasing the injection flow rate of the fracturing pump step by step (step pressure ≤ 5 MPa) at the start and stop stages of fracturing; the control of the pump pressure during the whole process of fracturing is within 70 MPa, which can prevent the casing deformation.

1. Introduction

The world is rich in unconventional oil resources. In 2002, the United States began to try horizontal well fracturing technology in unconventional gas reservoirs and began to promote horizontal well fracturing technology in 2007. In 2009, the completion of horizontal wells in the United States exceeded 95%, and the production reached 87.8 billion m³, accounting for about 15% of the natural gas production in that year, realizing the shale gas revolution. In 2013, the application rate of horizontal well bridge plug volume fracturing technology in North America reached 85% [1]; in 2010, PetroChina Tuha oilfield cooperated with American

Hess company to develop STH tight oil, continuously enriched the connotation of volume fracturing in the process of practical application [2], formed the main transformation process of “horizontal well bridge plug volume fracturing technology,” and realized the rapid production of unconventional oil and gas.

Tight oil M56 in the STH basin is a national tight oil area of demonstration. It is located at the ND No. 2 tectonic reservoir zone in Malang-sag; the reservoir extends to the east and west, high in the north, and low in the south, forming a trap area of 37.06 km²; the effective thickness of the reservoir is 51.3~52.9 m, the porosity is 9.90%~12.04%, and the permeability is 28.25~35.02 mD. The geostress includes the

stress caused by the weight of overburden rock and the modern tectonic stress transmitted from the adjacent block or bottom; it also includes the residual stress left by the past tectonic movement but not completely relaxed, as well as the stress change caused by nearby human engineering [3–6]. M56 reservoir adopts “horizontal well+casing+segmented volume fracturing technology,” realizing rapid scale benefit development. With the increasing demand for fracturing technology in the reservoir, the depth of reservoir and the length of the horizontal well are increasing; the key parameters of fracturing technology, such as “fracturing displacement, sand-adding strength, fluid volume, number of fracturing sections, and clusters,” have been continuously strengthened [7, 8], and the balance of the reservoir stress field is broken down and complex changes occur [9–11]; affected by the changes in the stress field, the reservoir casing is damaged to various degrees, and the problem of wellbore casing deformation caused by volume fracturing in horizontal wells is becoming more and more complex, showing an increase trend every year [12–14]. The casing deformation rate of shale oil and gas development reached 20%~30%, that of Marcellus shale oil well in the United States was 6.2%, that of Vaca Muerta shale gas well in Neuquén Basin in Argentina was 25%, that of a block in Duvernay in Canada was 47% [15], and the average casing deformation rate of shale gas horizontal wells in Changning, Wei 202, Wei 204, and Zhaotong blocks in China reached 38.46% by the end of 2019. The casing deformation rate of horizontal wells in M56 tight oil block in STH basin has also increased significantly. By the end of 2020, the casing damage rate of the horizontal wells in M56 has reached to 30%, which has affected the development of the STH M56.

In this paper, with rock mechanics experiments and statistical analysis methods of typical wells, we determined the geostress accurate data of the STH M56 basin and established the near-wellbore area geostress model. With the finite element analysis, the change characteristics of the near-wellbore geostress field of oil wells in M56 during fracturing are further studied and analyzed, and the preventive measures for volume fracturing in this area in terms of perforation mode and safe injection pump pressure are given. Through the application examples of 15 wells, it further explains the effectiveness of the measures.

2. Stress Calculation

2.1. Core Experiment

2.1.1. Tensile Test. *Test piece:* diameter $\Phi 25$ mm and thickness 6 mm~8 mm, see Figure 1.

Principle: Brazilian test, the test specimens are loaded through the two arc clips until the rock is split and damaged. The tensile strength of the rock is calculated through the load value when the test specimens are damaged.

$$\sigma_t = \frac{2P}{\pi Dt}, \quad (1)$$

where σ_t is the tensile strength, MPa; P is the load at fracture

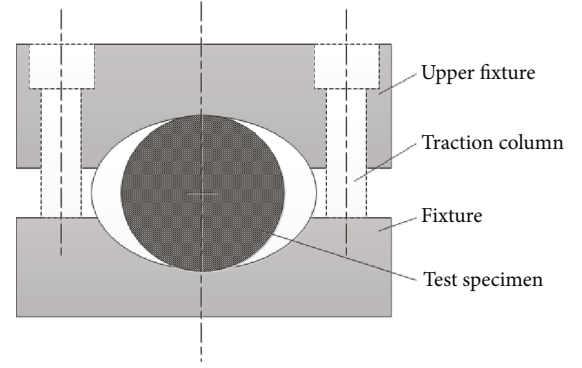


FIGURE 1: Diagram of rock and experimental principle.

of test specimens, N; D is the diameter of test specimens, mm; and t is the thickness of test specimens, mm.

2.1.2. Compression Test. *Test piece:* diameter $\Phi 25$ mm, length 50 mm.

Principle: draw the stress-strain curve with a triaxial compression test. Black line represents the axial strain stress, green line represents the radial strain stress, and the red line represents the volumetric strain stress, see Figure 2.

Compressive strength: the point of max-stress is the compressive strength σ_u .

$$\sigma_u = \frac{P}{A_0}, \quad (2)$$

where σ_u is the compressive strength, MPa; P is the axial load, N; and A_0 is the cross sectional of the initial test specimens, mm^2 .

Elastic modulus: the slope of the straight line at the half of the compressive strength is the elastic modulus.

$$E = \frac{\Delta\sigma_{50\%}}{\Delta\varepsilon_1}, \quad (3)$$

where E was Elastic modulus, MPa; $\Delta\sigma_{50\%}$ is the axial stress difference, MPa; and $\Delta\varepsilon_1$ is the axial strain difference, dimensionless.

Poisson's ratio: ν , the inverse of the ratio of the slope of the straight line at the half of the compressive strength is Poisson's ratio.

$$\nu = \frac{\text{midpoint slope of axial deformation curve}}{\text{midpoint slope of radial deformation curve}}. \quad (4)$$

2.2. Core Parameter Fitting. Core experiment reflects the physical and mechanical properties of rocks and pressure characteristics to a certain extent [16–18]. Through 120 core test experiments (see Figure 3), the elastic modulus and Poisson's ratio of cores in the M56 are obtained (see Figures 4 and 5). Using the statistical probability method was done to obtain the normal distribution of the probability curve and fitting equation of the horizontal stress ratio, stress difference distribution probability curve, and polynomial fitting equation (see Figures 6 and 7).

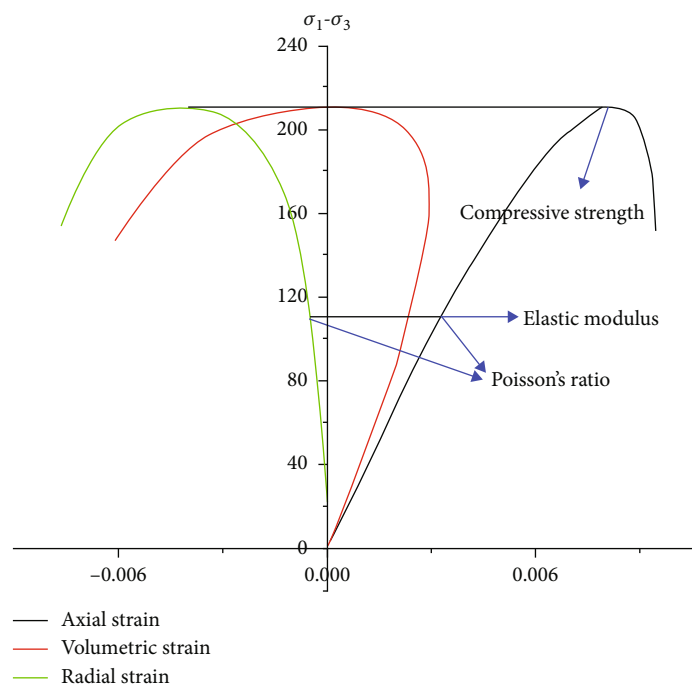


FIGURE 2: Schematic diagram of stress-strain curve.






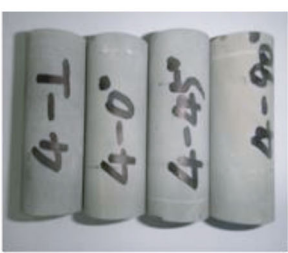


Tensile test	Before		
	After		
Compression test	Before		
	After		

FIGURE 3: Comparison diagram of rock slices before and after test.

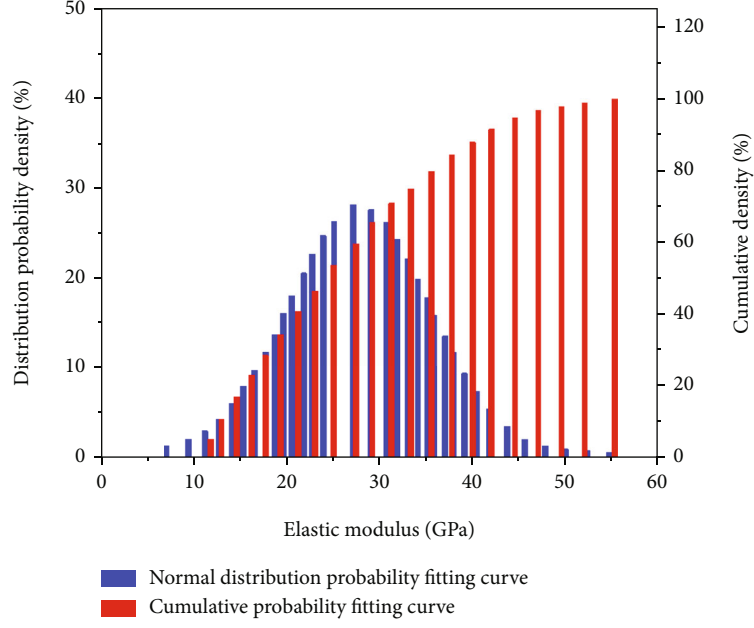


FIGURE 4: Probability distribution and fitting curve of the elastic modulus.

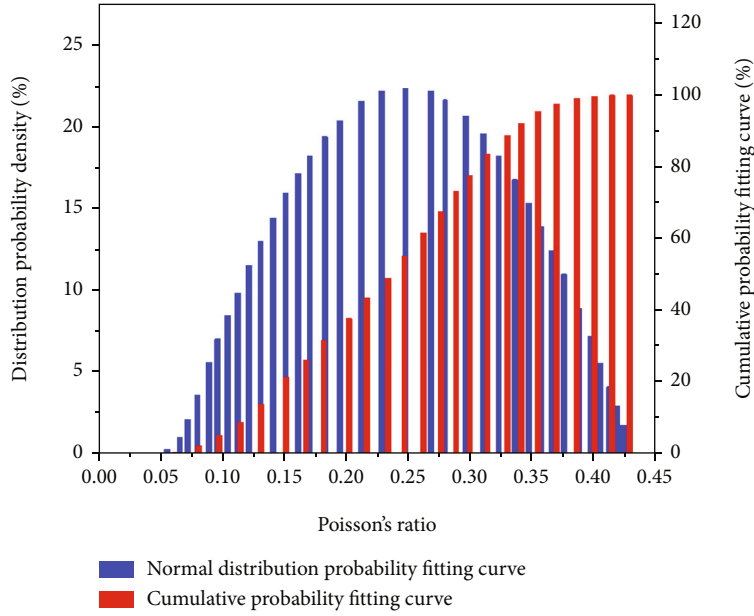


FIGURE 5: Probability distribution and fitting curve of Poisson's ratio.

Fitting equation of elastic modulus and probability distribution curve:

$$P_E = 0.69452 + \frac{558.74181}{16.27603 \times (\pi/2)^{1/2}} \times e^{-2 \times ((E-27.32837)/16.27603)^2},$$

$$R^2 = 0.8879,$$
(5)

where P_E is the elastic modulus, E is the coefficient of determination, and R^2 is the coefficient of determination.

From the probability fitting curve of elastic modulus distribution, the elastic modulus of the reservoir in the M56 conforms to the normal distribution, the coefficient of determination (R^2) is 0.8879, and it has high goodness of fit. The elastic modulus of rock core is concentrated at 20~30 GPa.

Fitting equation of Poisson's ratio and probability distribution curve:

$$P_\mu = -86.17334 + \frac{70.05168}{0.51456 \times (\pi/2)^{1/2}} \times e^{-2 \times ((\mu-0.24867)/0.51456)^2},$$

$$R^2 = 0.8559,$$
(6)

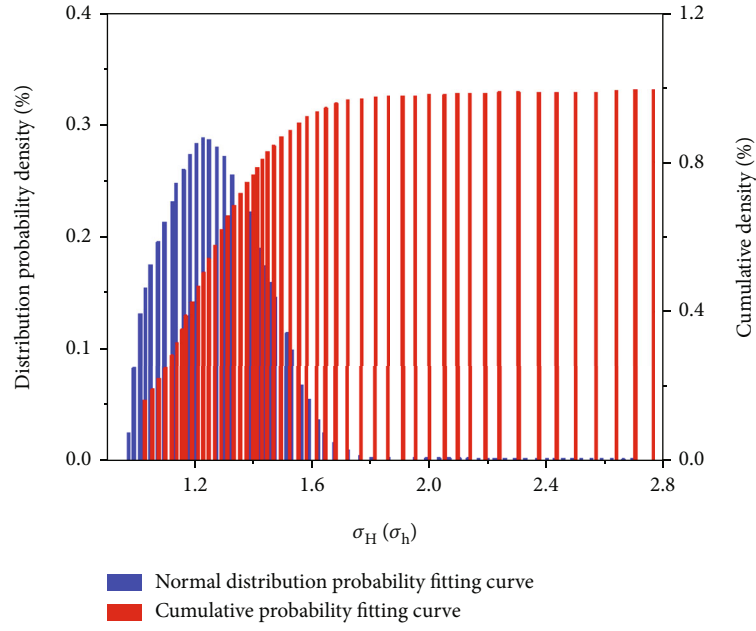


FIGURE 6: Probability distribution and fitting curve of the horizontal stress ratio.

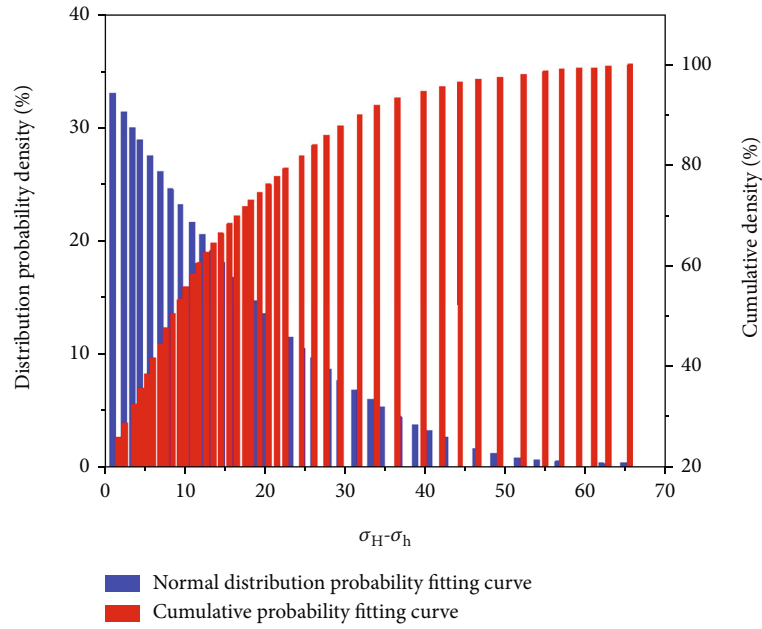


FIGURE 7: Probability distribution and fitting curve of the horizontal stress difference.

where P_μ is the distribution probability density, μ is Poisson's ratio, and R^2 is the coefficient of determination.

From the probability fitting curve of Poisson's ratio distribution, Poisson's ratio of the reservoir in the M56 conforms to the normal distribution, the coefficient of determination (R^2) is 0.8559, and it has high goodness of fit. Poisson's ratio of rock core is less than 0.25.

Fitting equation of horizontal stress ratio and probability distribution curve:

$$P_M = 0.0029 + \frac{0.13569}{0.38024 \times (\pi/2)^{1/2}} \times e^{-2 \times ((M-1.28928)/0.38024)^2}, \quad (7)$$

$$R^2 = 0.9938,$$

where P_M is the distribution probability density, $M = \sigma_H/\sigma_h$, and R^2 is the coefficient of determination.

From the probability fitting curve of horizontal stress ratio distribution, the horizontal stress ratio of the reservoir in the M56 conforms to the normal distribution, the coefficient of determination (R^2) is 0.9938, it has high goodness of fit, and the average horizontal stress ratio of the reservoir is concentrated at 1.2.

Polynomial fitting equation of the stress difference and probability distribution curve:

$$P_D = 34.77283 - 1.34694D + 0.0164D^2 - 5.68697 \times 10^{-5}D^3, \\ R^2 = 0.9542, \quad (8)$$

where P_D is the distribution probability density, $D = \sigma_H - \sigma_h$, and R^2 is the coefficient of determination.

From the probability fitting curve of horizontal stress difference distribution, the horizontal stress difference of the reservoir in the M56 conforms to the normal distribution, the coefficient of determination (R^2) is 0.9542, the goodness of fit is high, and the reservoir horizontal stress difference is concentrated at 6.1~7.6 MPa.

The results show that the distribution of rock parameters in the M56 tight oil conforms to the normal distribution, the coefficient of determinable (R^2) of the fitting equation ranges from 0.8559~0.9938, the goodness of fit is high, and the elastic modulus is 2.7×10^4 MPa. Poisson's ratio is less than 0.25, while the maximum and minimum horizontal principal stress ratio is 1.2, and the stress difference is 6.1~7.6 MPa (≤ 8 MPa). This characteristic condition is more conducive to the formation of complex fracturing network in the reservoir during fracturing.

2.3. Calculation of the Reservoir's Mechanical Parameters at Different Formation Depth. During fracturing, the circumferential stress of rock being squeezed by a high-pressure fracturing fluid should exceed its tensile strength in order to produce fractures, which can accurately reflect the formation stress. With the use of the 32 fracturing well parameters in tight oil STH M56, and with accord to the multiconstraint stress fine analysis technology [19], stress of the reservoirs at different formation depths is obtained (see Figure 8).

The resulting mathematical expression for stress:

$$\begin{aligned} \sigma_H &= -10.5 + 0.026H, \\ \sigma_h &= -5.87 + 0.020H, \\ \sigma_V &= (0.021 \sim 0.022)H, \end{aligned} \quad (9)$$

where σ_H is the maximum horizontal stress, σ_h is the minimum horizontal stress, σ_V is the vertical stress, and H is the formation depth.

The results show that the formation fracture pressure gradient of the tight oil M56 is 0.023~0.025 MPa/m, the maximum horizontal stress gradient is 0.025~0.026 MPa/m, the minimum horizontal stress gradient is 0.0198 MPa/m,

the max/min-horizontal stress ratio of 2000~2500 m is 1.20, and the vertical stress is greater than the minimum horizontal stress, that is, $\sigma_H > \sigma_V > \sigma_h$, consistent with the indoor test results in 1.2.

3. Modeling the Stress of the Near-Wellbore Horizontal Well

The stress of the near-wellbore horizontal well is composed of the stress under the geostress; the stress is caused by the pressure of the wellbore and formed by the fluid flowing into the formation [20–23]. The stress model of the near wellbore is established by using a linear elastic calculation model and superposition principle (see Figure 9).

3.1. Stress near the Wellbore under Geostress. The plane stress model is used to calculate the stress of the formation, the circumferential stress σ_θ , radial stress σ_r , vertical stress σ_z , and wellbore shear stress $\tau_{r\theta}$ that are caused by stress that are as follows:

$$\begin{aligned} \sigma_\theta &= \frac{\sigma_{Hmax} + \sigma_{Hmin}}{2} \left(1 + \frac{r_a^2}{r^2} \right) - \frac{\sigma_{Hmax} - \sigma_{Hmin}}{2} \\ &\quad \cdot \left(1 + \frac{3r_a^4}{r^4} \right) \cos 2\theta, \\ \sigma_r &= \frac{\sigma_{Hmax} + \sigma_{Hmin}}{2} \left(1 - \frac{r_a^2}{r^2} \right) + \frac{\sigma_{Hmax} - \sigma_{Hmin}}{2} \left(1 - \frac{r_a^2}{r^2} \right) \\ &\quad \cdot \left(1 - \frac{3r_a^4}{r^4} \right) \cos 2\theta, \\ \sigma_z &= \sigma_v - \nu \left[2(\sigma_{Hmax} - \sigma_{Hmin}) \frac{r_a^2}{r^2} \cos 2\theta \right], \\ \tau_{r\theta} &= \frac{\sigma_H - \sigma_h}{2} \left(1 - \frac{3r_a^4}{r^4} + \frac{2r_a^2}{r^2} \right) \sin 2\theta, \end{aligned} \quad (10)$$

where ν is Poisson's ratio of rock, dimensionless; r is the distance from the wellbore center, m; r_a is the borehole radius, m; θ is the included angle between radial and axial directions, °; σ_v is the overburden pressure, MPa; σ_{Hmax} is the max-horizontal principal stress, MPa; σ_{Hmin} is the min-horizontal principal stress, MPa; and $\tau_{r\theta}$ is the shaft shear stress, MPa.

3.2. Stress near the Wellbore under Internal Pressure. During fracturing, the pressure of the wellbore has complex changes. Assuming that the casing, the cement sheath, and formation are a continuum with no cracks, the stress field around the wellbore is solved with the use of the thick wall wellbore theory of elasticity. The circumferential stress σ_θ and radial stress σ_r are caused by hydraulic fracturing:

$$\begin{aligned} \sigma_\theta &= \frac{(P_e - P_i)r_e^2r_a^2}{(r_e^2 - r_a^2)r^2} + \frac{P_e r_e^2 - P_i r_a^2}{r_e^2 - r_a^2}, \\ \sigma_r &= \frac{r_a^2}{r^2} P_i, \end{aligned} \quad (11)$$

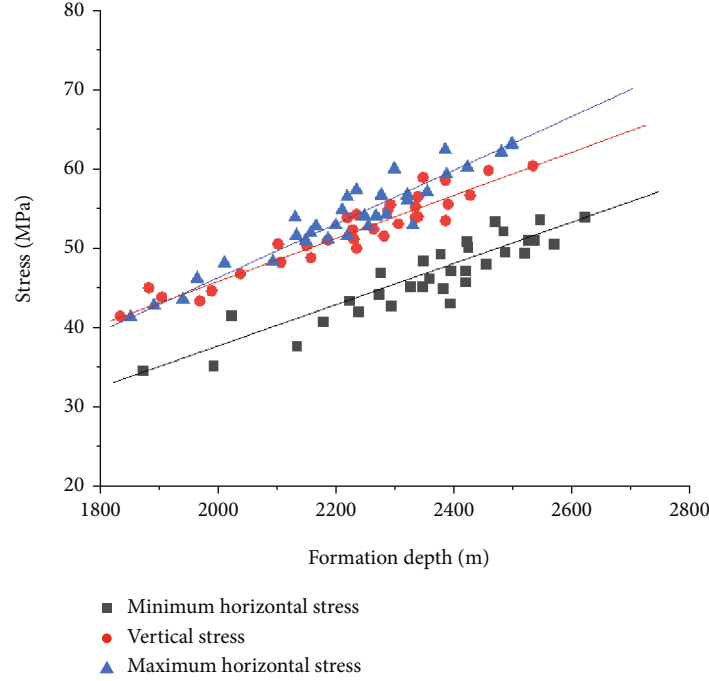


FIGURE 8: Relationship between the stress and the formation depth.

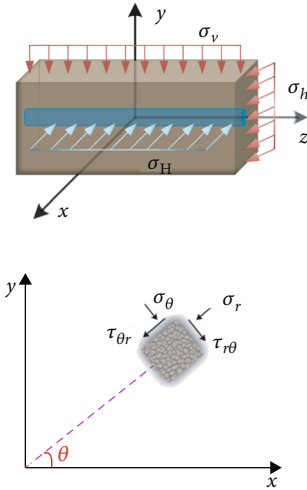


FIGURE 9: Stress model near the wellbore of horizontal well.

where P_e is the pressure of outer boundary wellbore, MPa; P_i is the pressure of wellbore, MPa; r_e is the radius of outer boundary wellbore, m; r_a is the radius of the wellbore, m; and r is the distance from the wellbore center, m.

3.3. Additional Stress Caused by Fracturing Fluid. During the fracturing, fracturing fluid enters into the formation porous medium through the perforation hole to generate additional stress on the casing. Additional circumferential stress σ_θ , radial stress σ_r , and vertical stress σ_z formula are as follows:

$$\begin{aligned}\sigma_\theta &= k \left[\frac{\alpha(1-2\nu)}{2(1-\nu)} \cdot \frac{r^2 + r_a^2}{r^2} - \phi \right] (P_i - P_s), \\ \sigma_r &= k \left[\frac{\alpha(1-2\nu)}{2(1-\nu)} \cdot \frac{r^2 - r_a^2}{r^2} - \phi \right] (P_i - P_s), \\ \sigma_z &= k \left[\frac{\alpha(1-2\nu)}{2(1-\nu)} - \phi \right] (P_i - P_s),\end{aligned}\quad (12)$$

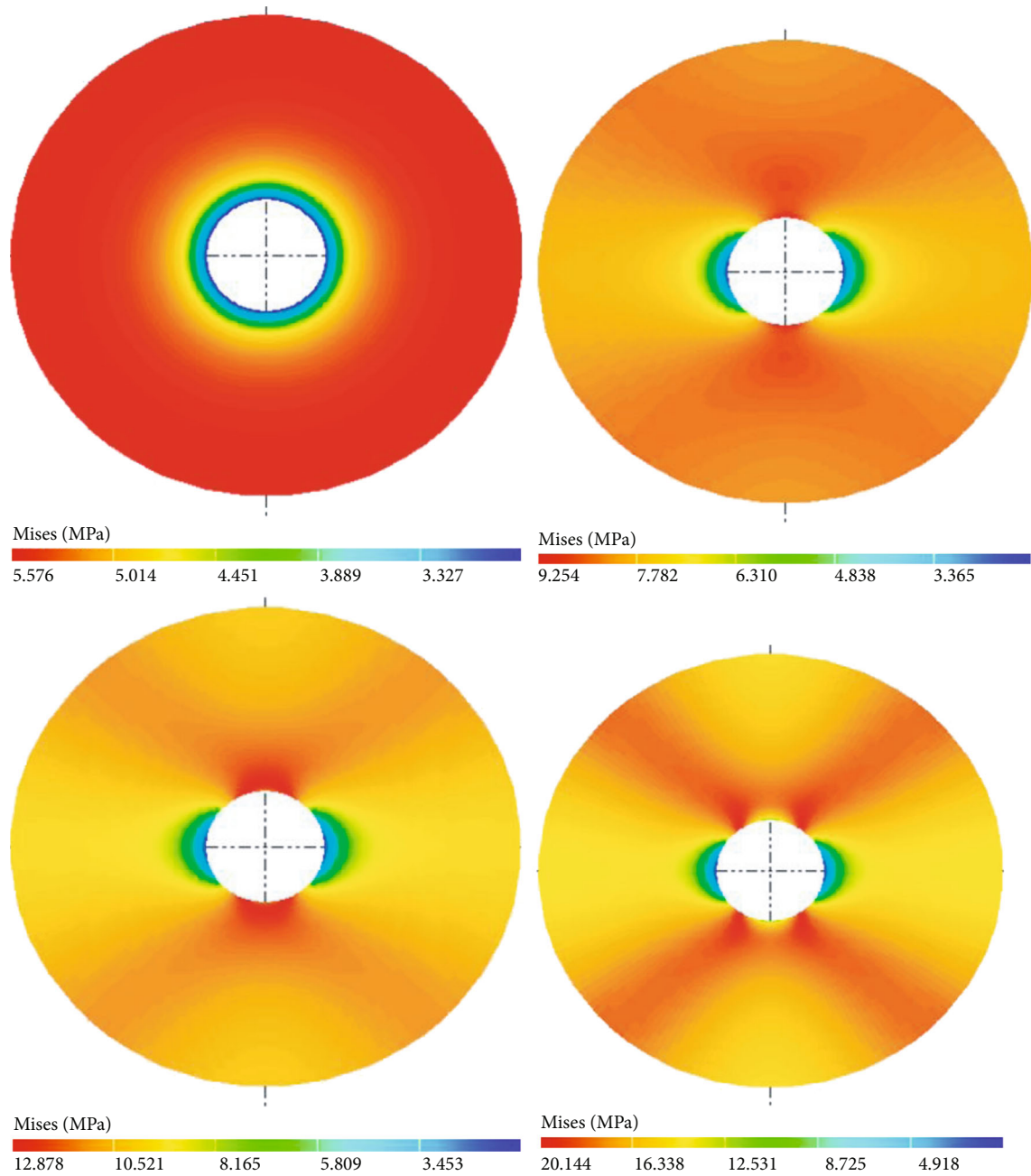
where ϕ is the porosity, 0~1; P_s is the pressure of rock pore, MPa; P_i is the pressure of wellbore, MPa; r is the distance from the wellbore center, m; and k is the dimensionless apparent permeability.

By coupling equations, obtain the expression of dimensionless apparent permeability as follows [24, 25]:

$$k = \frac{16d_m}{3d_p\eta} \left[\frac{3d_p}{16d_m} \eta + \frac{\sqrt{2}}{8} \left(\frac{2}{f} - 1 \right) + \frac{2\sqrt{2}}{3\pi} \frac{(1-\eta)^3}{(1+\eta+\eta^2-\eta^3)} \right], \quad (13)$$

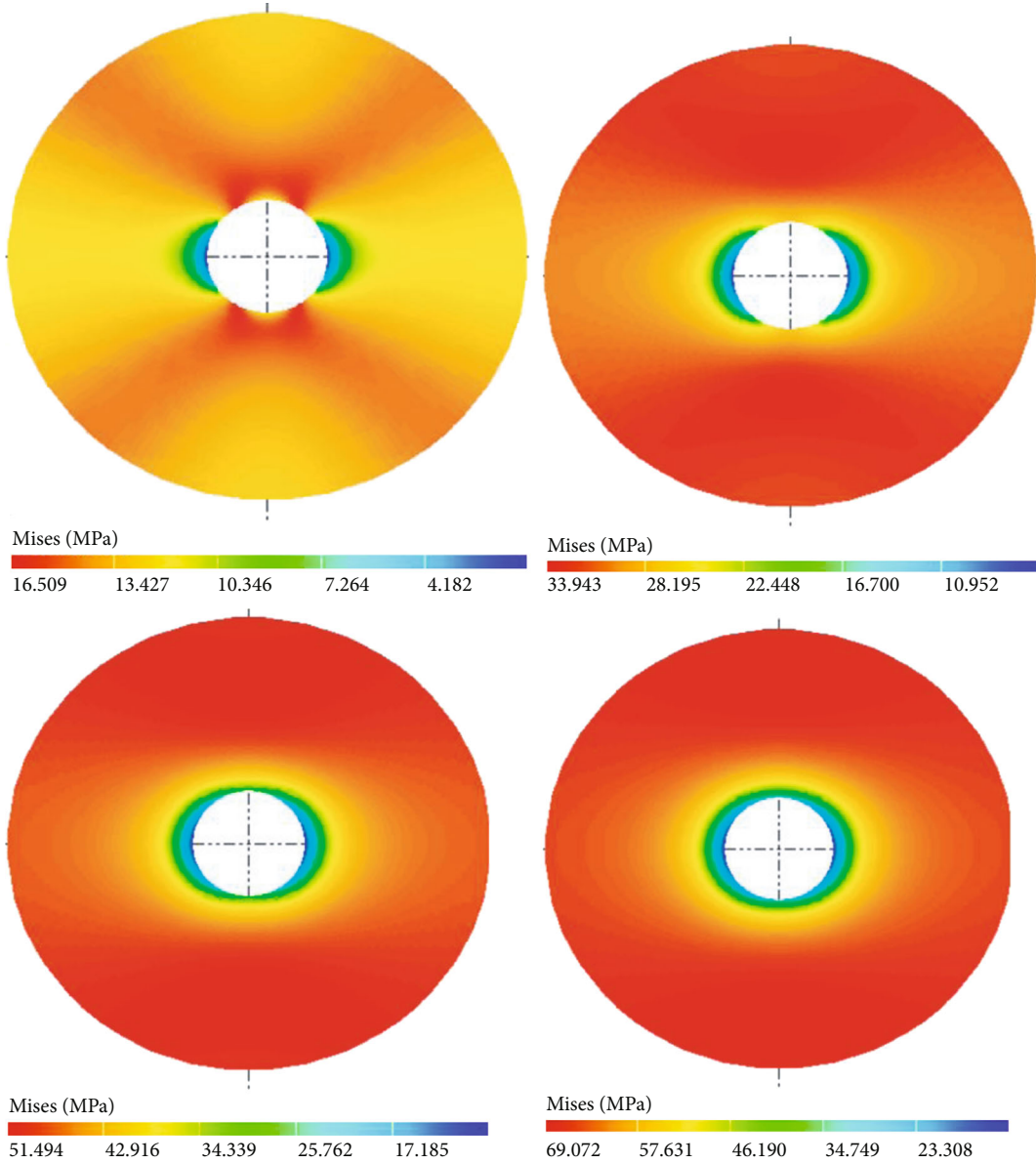
where d_m is the molecular diameter, m; d_p is the nanopore diameter, m; f is the tangential momentum accommodation coefficient (TMAC), dimensionless; and η is the packing fraction of the gas in the nanopore, dimensionless.

According to the superposition principle, the stress of formulas (10)–(13) ($r_e = \infty$, $r = r_a$, and $k = 1$) is superimposed to obtain a three-dimensional stress of the near horizontal wellbore:



(a) Uniformity coefficient 1.0, 1.1, 1.2, and 1.3 and fracturing pressure 40 MPa

FIGURE 10: Continued.



(b) Uniformity coefficient 1.2 and fracturing pressure 40, 50, 60, and 70 MPa

FIGURE 10: Mises stress near the wellbore under the uniformity coefficient-fracturing pressure.

$$\begin{aligned}
 \sigma_{\theta} &= \sigma_{Hmax} + \sigma_{Hmin} - 2(\sigma_{Hmax} - \sigma_{Hmin}) \cos 2\theta - P_i \\
 &\quad + \frac{\alpha(1-2\nu)}{1-\nu} (P_i - P_s), \\
 \sigma_r &= P_i, \\
 \sigma_z &= \sigma_v - 2\nu(\sigma_{Hmax} - \sigma_{Hmin}) \cos 2\phi + \frac{\alpha(1-2\nu)}{2(1-\nu)} (P_i - P_s).
 \end{aligned}
 \tag{14}$$

4. Stress Characteristic Analysis and Preventive Measures near the Wellbore

Taking the typical well of STH M56 as an example, the Mises stress characteristics of near the wellbore are analyzed, and

technical measures of the prevent casing deformation are formulated. The casing parameters of oil wells in this reservoir are as follows: outside diameter 139.7 mm, steel grade P110, thickness 9.17 mm, inner diameter 121.36 mm, long circular thread, and minimum internal yield strength of 90.7 MPa, and the mechanical parameters of the reservoir are calculated under the experimental and simulation data.

4.1. Mises Stress Characteristic Analysis. Results show that (1) the value of uniformity coefficient ($\mu_d = \sigma_{Hmax} / \sigma_{Hmin}$) is getting bigger and bigger, the more difference in the distribution isopleth of Mises stress. The horizontal stress of the near wellbore gradually decreases along the radial direction, the vertical stress of the near wellbore first increases and then decreases, four stress concentration points are

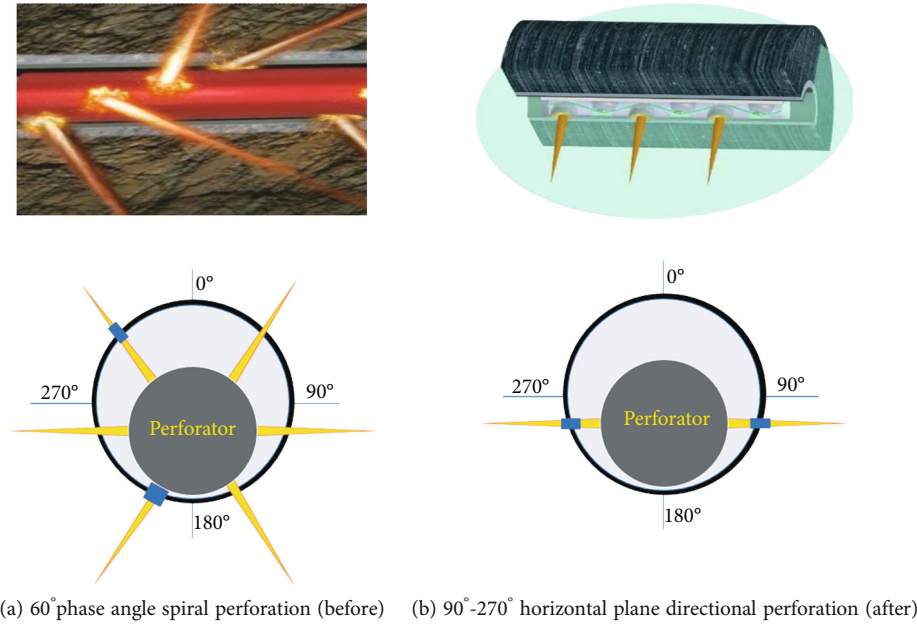


FIGURE 11: Comparison diagram of before and after perforation optimization.

symmetrically distributed near the borehole, and the max-stress point is perpendicular to the borehole axis, forming a high stress zone along the borehole radial direction, see Figure 10(a). The uniformity coefficient of the STH M56 reservoir is 1.2; it is seen that there are high stress points in the following directions of the casing, 30°, 150°, 210°, and 330°. When the casing strength is further reduced, these high stress points are the initial danger points for casing deformation. (2) Mises stress isopleth of the vertical and horizontal is being reversed with the pressure increase of the wellbore, the vertical stress first increases and then decreases, and the horizontal stress first decreases and then increases, see Figure 10(b).

Preventive measures: (1) the conventional 60° phase angle spiral perforation method has two shortcomings. First, the perforation angle can easily reduce the strength of the casing near the dangerous point, with increased risk of casing deformation. Second, because the perforator cannot be centered in the casing, the diameter of perforation hole at the top part of the casing is smaller than that at the bottom part, and the uneven perforation results in uneven liquid inflow during fracturing, because the direction of the formation fracture expansion and extension is mainly determined by the direction of the natural fracture principal stress; the fractures start from the weakest point during fracturing, most fluid enters the bottom large hole of the casing with low friction, and the strength of the casing at the bottom is further reduced, increasing the risk of casing deformation, see Figure 11(a); at the same time, the number of effective holes for fracturing fluid injection is reduced, which affects the fracturing effect. In view of the four high stress dangerous points in casing and near the borehole during fracturing in STH M56, the horizontal fixed plane perforating mode is proposed, which adopts 90° and 270° horizontal direction perforating, effectively avoiding the four high stress danger zones of the casing and greatly reducing the risk of casing strength decline at the high stress position

caused by perforating; it can also perforate along the direction of the maximum principal stress; the fracturing fracture first starts just along the direction of the maximum principal stress and extends outward, improving the fracturing effect, see Figure 11(b). (2) According to the vertical and horizontal Mises stress reverses with the increase of wellbore pressure, the fracturing of the M56 is prone to casing horizontal deformation when there is low-pump injection pressure and casing vertical deformation when there is high-pump injection pressure. Therefore, during the beginning and the end of fracturing, a step pressure stabilization method is proposed to slowly increase and decrease displacement of fracturing (step pressure ≤ 5 MPa), especially when the fracturing pressure is 40 MPa; pressure stabilization requires no less than 5 min in duration, to avoid the rapid rise or fall of the wellbore pressure with the uneven release of casing stress, which can increase the risk of casing deformation.

4.2. Analysis of Mises Stress and Fracturing Pressure. Results show that the max-Mises stress at the borehole wall and stress uniformity coefficient follows a linear positive correlation function. When the fracturing pressure is 40 MPa, the max-Mises stress of the casing wall is at its smallest. When the fracturing pressure exceeds to 60 MPa, the max-Mises stress of the casing wall increases along with the increase of the fracturing pressure (see Figure 12). As the fracturing pressure increases, the higher the risk of casing deformation is. During the multistage fracturing, the casing is repeatedly subjected to alternating stress of high and low inside the wellbore, and when the wellbore internal pressure reaches the minimum casing yield strength, the risk of casing deformation will be greatly increased.

The stress uniformity coefficient of STH M56 basin is 1.2; when the fracturing pressure reaches to 80 MPa, the max-Mises stress of the casing wall is about 88~93 MPa, the minimum yield strength of oil well casing has been

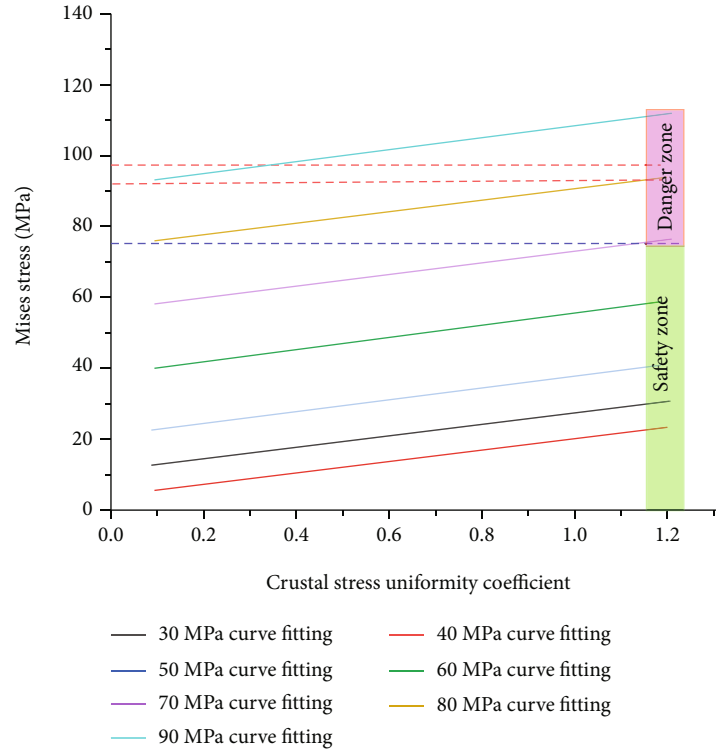


FIGURE 12: Curve of the borehole wall max-Mises stress and stress uniformity coefficient.

exceeded, and the minimum yield stress of the casing is 90.7 MPa (139.7 mm P110 casing and thickness 10.54 mm). It can be seen from Figure 12 that the fracturing pressure is 70 MPa and the max-Mises stress of the casing wall is 77 MPa, that is, 85% of the minimum casing yield strength, which is the reasonable pressure of the designed casing for fracturing and the safe fracturing pressure of oil wells in this block.

5. Field Experiments

According to the calculation results, field experiment study on staged fracturing of 15 horizontal wells in STH M56 tight oil was done through the application of “horizontal well+staged multicluster perforation” fracturing technology. The strength grade of casing is P110, the inner diameter is 121.36 mm, the vertical depth of horizontal well is 2380~2510 m, the number fracturing section of a well is 8~10, the section length of fracturing is 40~60 m, the fracturing section contains 6~8 clusters, the distance between the two clusters is 10~15 m, the fracturing fluid volume of each section is 1000~1100 m³, and the sand volume is 90~100 m³.

The 90° and 270° horizontal fixed plane perforations were used. During fracturing, with the start and stop of fracturing pump with step by step, the step pressure does not exceed 5 MPa. The increased displacement of fracturing pump is divided into five stages, 3, 6, 9, 11, and 12~15 m³/min; the pressure of every stage is stabilized for one minute. In the stopped stage, the reduced displacement of fracturing pump is divided into 15~12, 11, 9, 6, and 3~0 m³/min, and the pressure of every stage is stabilized for one minute. The maximum pressure of fracturing is 69.3 MPa (below design

safety pressure 70 MPa), the average pressure of fracturing is 65.7 MPa, and the displacement of fracturing is 8~12 m³/min. The field experiments indicate that no casing deformation happens during the fracturing and production within 1.5 years.

6. Conclusion and Suggestion

- (1) The stress reservoir of the STH M56 tight oil has a relationship of $\sigma_H > \sigma_V > \sigma_h$. The ratio of the horizontal maximum and minimum stress is 1.2, and the difference is less than 8 MPa. The elastic modulus is 2.7×10^4 MPa, and Poisson's ratio less than 0.25
- (2) According to the three-dimensional stress model of the near horizontal wellbore, in M56 basin, the Mises stress isoline near the well borehole is symmetrically distributed and has four dangerous points of stress concentration; a sector-shaped high dangerous stress zone is formed along the four dangerous points. As the pumping pressure increases, the vertical Mises stress first increases and then decreases, while the horizontal Mises stress first decreases and then increases. The max-Mises stress at the casing wall is linearly and positively correlated with the stress uniformity coefficient. When fracturing pressure is 70 MPa, the Mises stress reaches the dangerous stress of the casing, so pressure of 70 MPa fracturing is the safe pumping pressure for the reservoir casing
- (3) The 15 fractured wells in the M56 are perforated at 90° and 270° in the horizontal fixed plane perforation, and

the step type (step pressure ≤ 5 MPa) increase or decrease displacement of the fracturing is used during the start and stop of the pump, and the injection pressure of the fracturing process is less than 70 MPa that can effectively prevent the casing deformation of the horizontal well in the M56

Data Availability

The data that support the findings of this study are available from the first author, Peng Zhang, upon reasonable request.

Conflicts of Interest

The authors declare that they have no conflicts of interest.

Acknowledgments

This work was supported by the National Natural Science Foundation of China (grant numbers 62173049 and 52104057), the Natural Science Foundation of Shandong Province (grant number ZR2021QE106), and the China Postdoctoral Science Foundation (grant number 2021 M693506).

References

- [1] Q. Wu, Y. Xu, S. Zhang et al., "The core theories and key optimization designs of volume stimulation technology for unconventional reservoirs," *Acta Petrolei Sinica*, vol. 35, no. 4, pp. 706–714, 2014.
- [2] Q. Wu, Y. Xu, X. Wang, T. Wang, and S. Zhang, "Volume fracturing technology of unconventional reservoirs: connotation, optimization design and implementation," *Petroleum Exploration and Development*, vol. 3, pp. 99–105, 2012.
- [3] Q. Liu, D. Wang, Y. Zhu, Z. Yang, and B. Yin, "Application of support vector regression algorithm in inversion of geostress field," *Rock and Soil Mechanics*, vol. 41, no. S1, pp. 319–328, 2020.
- [4] Y. Zhang and J. Zhang, "Lithology-dependent minimum horizontal stress and in-situ stress estimate," *Tectonophysics*, vol. 703–704, pp. 1–8, 2017.
- [5] K. Shin, K. Sugawara, and S. Okubo, "Application of Weibull's theory to estimating in situ maximum stress σ_H by hydrofracturing," *International Journal of Rock Mechanics and Mining Sciences*, vol. 38, no. 3, pp. 413–420, 2001.
- [6] J. S. Bell, "Practical methods for estimating in situ stresses for borehole stability applications in sedimentary basins," *Journal of Petroleum Science and Engineering*, vol. 38, no. 3–4, pp. 111–119, 2003.
- [7] H. Liu, S. Meng, J. Su, G. Zhang, and L. Chen, "Reflections and suggestions on the development and engineering management of shale gas fracturing technology in China," *Natural Gas Industry*, vol. 39, no. 4, pp. 1–7, 2019.
- [8] Y. Xu, Q. Lei, M. Chen et al., "Progress and development of volume stimulation techniques," *Petroleum Exploration and Development*, vol. 45, no. 5, pp. 874–887, 2018.
- [9] L. Zhuopei, N. Zhou, J. Cui, F. Jian, W. Zihong, and S. Wei, "Application of a new 3D geostress modeling technology in Changning deep shale gas block," *Drilling & Production Technology*, vol. 42, no. 6, pp. 5–8, 2019.
- [10] W. Zhengrong, D. Hui, and H. Runqiu, "Three-dimensional inversion of geostress in Xinchang gas field, Western Sichuan Sag," *Petroleum Geology & Experiment*, vol. 36, no. 6, pp. 792–797, 2014.
- [11] J. Li, M. Chen, G. Q. Zhang, and H. Zhang, "Analysis on stress distribution of casing in sloughing formation with finite element method," *Journal of the University of Petroleum, China (Edition of Natural Science)*, vol. 28, no. 2, pp. 45–48, 2004.
- [12] C. Zhaowei and C. Yongen, "Study on casing load in a casing-stratum system by elastoplastic theory," *Petroleum Exploration and Development*, vol. 36, no. 2, pp. 242–246, 2009.
- [13] T. Wang, R. Y. Jiang, Y. L. Han, J. H. Zhang, and Y. Zhang, "The casing failure mechanism in the ultra-deep horizontal well and research on the technology of the precaution, diagnose and treatment in H oilfield," *Journal of Southwest Petroleum University: Science & Technology Edition*, vol. 31, no. 1, pp. 156–161, 2009.
- [14] C. Z. Yan, H. Zheng, G. H. Sun, and X. R. Ge, "Effect of stress on hydraulic fracturing based on FDEM-flow," *Rock and Soil Mechanics*, vol. 37, no. 1, pp. 237–246, 2016.
- [15] P. Zhang, Y. He, Z. Liu et al., "Shear compression deformation test and deformation prevention practice of casing in shale gas horizontal wells," *Natural Gas Industry*, vol. 41, no. 5, pp. 84–91, 2021.
- [16] X. Fang and X. Xu, "Experimental and mechanism research about permeability damage with the change of stress," *Petroleum Exploration and Development*, vol. 29, no. 2, pp. 117–119, 2002.
- [17] M. Jianhai and S. Jianmeng, "Calculation of formation stress using logging data," *Well Logging Technology*, vol. 26, no. 4, pp. 347–351, 2002.
- [18] Y. Deng, J. Guo, and J. Zhao, "New method for calculating stress profile and its application," *Lithologic Reservoirs*, vol. 24, no. 2, pp. 124–127, 2011.
- [19] H. Fan, *Study on Casing Strength and Safety Reliability of Utupud Gas Wells*, China University of Petroleum (East China), 2016.
- [20] J. Liu, L. Chen, and J.-l. Wang, "Analysis of temperature stress characteristics of shaft lining," *Geotechnical Mechanics*, vol. 32, no. 8, pp. 2386–2390, 2011.
- [21] Z. She-rong, H. An-kui, W. Chao, and P. Zhen-hui, "Three-dimensional intelligent inversion method for in-situ stress field based on SLR-ANN algorithm," *Rock and Soil Mechanics*, vol. 38, no. 9, pp. 2737–2746, 2017.
- [22] B. Wang, S. Zhang, and L. Li, "Optimization design method of well pattern based on stress field," *Petroleum Geology & Oilfield Development in Daqing*, vol. 26, no. 3, pp. 55–59, 2007.
- [23] X. H. Qin, C. X. Tan, J. Z. Sun, Q. C. Chen, and M. J. An, "Experimental study of relation between in-situ crustal stress and rock elastic modulus," *Rock and Soil Mechanics*, vol. 33, no. 6, pp. 1689–1695, 2012.
- [24] J. Wang, H. Q. Liu, L. Wang, H. L. Zhang, H. S. Luo, and Y. Gao, "Apparent permeability for gas transport in nanopores of organic shale reservoirs including multiple effects," *International Journal of Coal Geology*, vol. 152, pp. 50–62, 2015.
- [25] J. Xu, K. Wu, S. Yang, J. Cao, and Z. Chen, "Nanoscale free gas transport in shale rocks: a hard-sphere based model," in *SPE Unconventional Resources Conference*, Calgary, Alberta, Canada, February 2017.